Theory and Simulations of Electrocatalyst-Coated Semiconductor Electrodes for Solar Water Splitting

Thomas J. Mills, Fuding Lin, and Shannon W. Boettcher*
Department of Chemistry and Biochemistry, University of Oregon, Eugene, Oregon 97403, USA
(Received 25 May 2013; revised manuscript received 20 February 2014; published 8 April 2014)

We develop a theory of charge transfer at semiconductor-catalyst interfaces to elucidate the current-potential behavior of semiconductor-catalyst-solution systems used for solar water splitting and compare simulations based on this theory to experimental data. Ion-permeable catalysts are found to form semiconductor-catalyst interfaces where the effective barrier height changes under operation yielding higher photovoltages and efficiencies relative to dense catalysts with the same catalytic activity. Such behavior is not captured by current equivalent circuit models, but is central to the study and design of efficient water-splitting systems.

DOI: 10.1103/PhysRevLett.112.148304 PACS numbers: 82.47.Jk, 73.30.+y, 73.40.Mr, 88.30.ep

Leading designs for photoelectrochemical water-splitting devices incorporate semiconductors coupled with electrocatalyst films in aqueous electrolytes [1]. A common model of such semiconductor-catalyst-solution (SCS) systems [Fig. 1(a)] comprises a semiconductor that absorbs light and separates charge in series with a catalyst that increases the rate of the hydrogen-evolution reaction or oxygen-evolution reaction (OER). Experiments, however, show that after deposition of OER catalysts onto *n*-type semiconductors, the photoelectrode characteristics—e.g., the photovoltage, photocurrent, and fill factor—change in a manner inconsistent with this simple model. Competing hypotheses have attributed this behavior to changes in surface recombination and/or band bending, interface charge trapping, and optical effects [2–7].

Designing efficient SCS devices requires clarifying the interface physics and the ability to discern between competing mechanisms. While the theory of semiconductor-electrolyte interfaces is well developed [8], it has not been rigorously extended to accommodate a catalyst on the semiconductor surface [9]. One major challenge is that OER catalysts are complex materials with variable properties, such as porosity or ion permeability and redox energy levels or electronic density of states (DOS).

We develop a theory of SCS systems that accounts for the kinetics of charge transfer between semiconductor, catalyst, and solution, for ion-permeable and ion-impermeable catalysts with either an extended or localized electronic DOS [9]. We apply this theory using numerical simulations to predict the behavior of illuminated *n*-type semiconductor photoelectrodes in contact with three different types of catalysts. We refer to these catalysts as *metallic*, *adaptive*, or *molecular*, each of which represents a class of experimentally relevant OER catalysts. We find that the predicted photoresponse depends dramatically on the ion permeability and electronic DOS of the catalyst, which is unexpected based on the traditional view of semiconductor-catalyst interfaces but consistent with our recent experiments [9,10]. This work therefore provides a new conceptual framework for studying and optimizing SCS systems.

We define metallic catalysts as those with a continuum of electronic states (as in a free-electron model [9]) and no ion permeability. Examples of such catalysts are crystalline IrO_x and Pt/PtO [11]. SCS systems with metallic catalysts function as "buried" junctions [12,13]; that is, electron transport between semiconductor and catalyst is independent of the catalyst potential. These systems are described well by the series equivalent circuit shown in Fig. 1(a). This approach has been used to model catalyst-coated Si *pn*

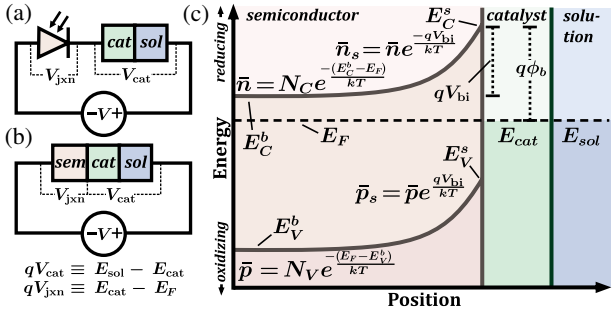

FIG. 1 (color online). (a) Simple equivalent circuit of a semiconductor-catalyst-solution (SCS) system where the semiconductor is treated as a separate photodiode element. (b) Generalized equivalent circuit model where all three subsystems are treated as a single element. (c) Equilibrium energy diagram of an SCS system, defining: the solution potential E_{sol}, the catalyst potential E_{cat}, the conduction and valence band edges E_C and E_V, the bulk electron and hole concentrations $\bar{n}$ and $\bar{p}$ (where N_C and N_V are the effective DOS constants of the conduction and valence bands), and the equilibrium electron and hole surface concentrations $\bar{n}_s$ and $\bar{p}_s$. In the metallic model, E_{cat} is fixed relative to E_C^s and E_V^s, whereas it is free to move in the adaptive and molecular models.

junctions [14,15] and semiconductor electrodes modified with redox-active molecules [16].

Many high-activity OER catalysts, however, are not dense solids, but instead hydrous transition metal oxides, hydroxides, or oxyhydroxides [17–19]. These catalysts often exhibit broad redox waves associated with an extended DOS, bulk oxidation or reduction, and free movement of ions throughout the catalyst. We define catalysts with these properties as adaptive because, as we show below, the effective barrier for electron transfer at the semiconductor-catalyst interface increases as the catalyst is oxidized to its operational state. Related phenomena are observed in conjugated-ionomer systems [20].

We define molecular catalysts to have a narrow electronic DOS localized at a single redox energy, as with an idealized molecular redox couple [21,22]. Molecular catalysts are studied for attachment to semiconductor surfaces as monolayers [23]. Because molecular monolayers are thin, they are considered to be ion permeable.

The ion-permeable adaptive and molecular catalysts cannot be modeled by the previously used series circuit [4,13–16] shown in Fig. 1(a) and are thus represented here by the generalized circuit in Fig. 1(b). Simulations based on our new model show that SCS systems containing ion-permeable catalysts compensate for slow catalyst rate constants by shifting the catalyst potential relative to the semiconductor band edges.

We use the semiconductor sign convention (higher electron energy is more positive) except for the applied, semiconductor, and catalyst potentials, so that generated $J(V)$ curves are consistent with electrochemical experiments. We model an n-type semiconductor with an Ohmic back contact. Referencing to the solution potential $E_{\mathrm{sol}} \equiv 0$ eV, we chose isolated semiconductor conduction and valence bands of $E_C^0 \equiv 1$ eV and $E_V^0 \equiv -1$ eV, and an isolated semiconductor Fermi level $E_F^0 \equiv 0.75$ eV, with majority carrier concentration $\bar{n} \approx 6 \times 10^{15}$ cm^{-3}. The solution contains a one-electron redox couple with a potential E_{sol} in the middle of the semiconductor band gap, which is roughly the position of the O_2/OH^- couple relative to the band edges of oxide photoanodes [24]. The use of a one-electron couple is a simplification of the four-electron O_2/OH^- couple, but captures the essential mechanisms and does not affect the conclusions drawn.

The recombination rate was set such that the quantum efficiency was ≈0.97 at applied bias $V \equiv (E_{\mathrm{sol}} - E_F)/q = 0$ (short circuit). The photon flux was set to 10^{17} cm^{-2} s^{-1}, roughly equivalent to one sun. We assume no catalyst optical absorption, giving a photocurrent of ≈15.5 mA cm^{-2} at $V = 0$. Other parameters used in the simulation are listed in the Supplemental Material [9], as well as descriptions of the models and simulation techniques [9]. The drift-diffusion, continuity, and Poisson's equations, coupled to boundary conditions defined below, are numerically solved to obtain the steady-state carrier profiles, electrostatic potential profiles, catalyst potential E_{cat}, and current density J.

Figures 1(a) and 1(b) show the chemical potential differences across the semiconductor $qV_{\mathrm{jxn}} \equiv E_{\mathrm{cat}} - E_F$, and the catalyst $qV_{\mathrm{cat}} \equiv E_{\mathrm{sol}} - E_{\mathrm{cat}}$ (i.e., the kinetic overpotential). Figure 1(c) shows an energy diagram of an ideal SCS system at equilibrium and defines parameters used in the text. We assume constant concentrations of redox species O and R, so E_{sol} does not deviate from its equilibrium value, as is the case with the O_2/OH^- couple where $[OH]^-$ is large and O_2 is saturated.

For ion-permeable catalysts there is no electrostatic potential drop in the catalyst or solution because the electrolyte screens any field in these materials. The applied potential thus develops across the semiconductor. In contrast, with impermeable (metallic) catalysts, a portion of the electrostatic potential must drop at the catalyst-solution interface in order to drive the reaction.

We begin with metallic catalysts. To facilitate comparison with the other models, we set the Fermi level of the metal catalyst equal to E_{sol}, so that there is no potential drop between the catalyst and solution at equilibrium. The current is written in terms of equilibrium ($\bar{n}_s$, $\bar{p}_s$) [see Fig. 1(c)] and nonequilibrium (n_s, p_s) surface carrier concentrations [9],

$$J_{\mathrm{jxn}} = k_p(p_s - \bar{p}_s) - k_n(n_s - \bar{n}_s), \tag{1}$$

where k_p and k_n are forward rate constants for hole and electron transfer, respectively, between the semiconductor and metal. The first term represents forward and backward hole currents, the second forward and backward electron currents. This boundary condition was used to obtain the $J(V)$ response of the photodiode circuit element. The simulated photodiode response was well approximated by the ideal photodiode equation, $J_{\mathrm{jxn}} \approx J_{\mathrm{ph}} - k_n\bar{n}_s(e^{-qV_{\mathrm{jxn}}/kT} - 1)$, which results from assuming a constant hole photocurrent J_{ph} and quasiequilibrium of electrons.

We use Butler-Volmer kinetics to model electron transfer between the catalyst and the redox couple,

$$J_{\mathrm{cat}} = J_{\mathrm{o,cat}}(e^{qV_{\mathrm{cat}}/2kT} - e^{-qV_{\mathrm{cat}}/2kT}), \tag{2}$$

where we have taken the transfer coefficient to be 1/2. $J_{\mathrm{o,cat}}$ is the exchange current density. The Tafel slope is 118 mV decade^{-1} at 25 °C.

The $J(V)$ response of the metallic model was obtained by using the current ($J = J_{\mathrm{jxn}} = J_{\mathrm{cat}}$) and potential drop ($V = V_{\mathrm{jxn}} + V_{\mathrm{cat}}$) equality conditions for series circuits. Combining these conditions with the $J(V)$ responses of the two circuit elements yielded J and V_{cat} for a range of $J_{\mathrm{o,cat}}$ values [Figs. 2(a) and 2(b)]. When the catalyst is fast (i.e., $J_{\mathrm{o,cat}}$ is large), $V_{\mathrm{cat}} \approx 0$ and the total response is that of the photodiode.

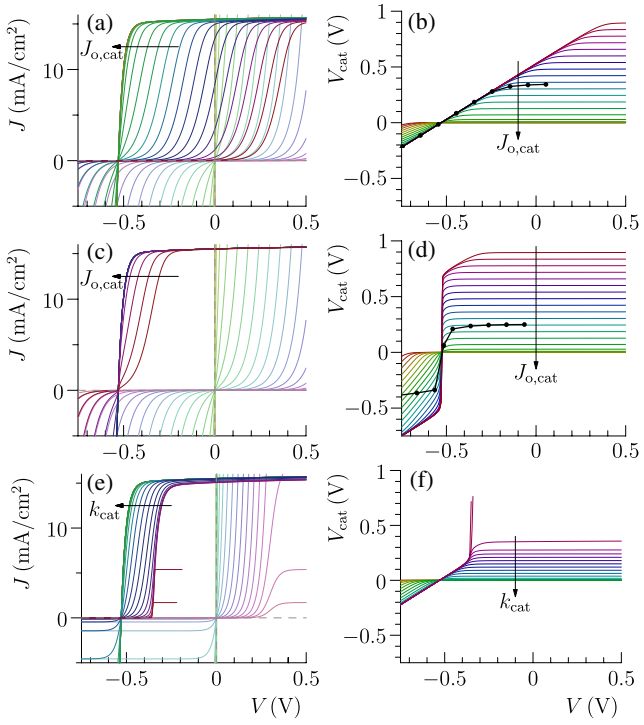

FIG. 2 (color online). J and V_{cat} curves for the metallic [(a),(b)], adaptive [(c),(d)], and molecular [(e),(f)] models, for a range of $J_{o,cat}$ and k_{cat} values—each color corresponds to a single value of $J_{o,cat}$ or k_{cat}. The colors in each subfigure correspond to equivalent values of $J_{o,cat}$ and k_{cat}. $J_{o,cat}$ ranges from 1.4×10^{7} to 1.4×10^{-4} mA cm^{-2}, and the values of k_{cat} used were $J_{o,cat}(1+K)/\hat{C}$ (*vide infra*). Arrows indicate increasing values of $J_{o,cat}$ and k_{cat}. The black points show experimental values of V_{cat} for nanocrystalline IrO_x (b) and hydrous $Ni(OH)_2/NiOOH$ (d) catalysts on n-TiO_2 [10], with V shifted to account for different photovoltages. In (a), (c), and (e), the $J(V)$ responses of the system are shown in bold lines, and the responses of the isolated catalyst [Eq. (2) for (a) and (c), Eq. (6) for (e)] are shown in dim lines.

When the catalyst is slow (and $J < J_{ph}$), $V_{cat} \approx V - V_{oc}$ (V_{oc} is the open-circuit voltage), the $J(V)$ response becomes

$$J \approx J_{o,cat}(e^{q(V-V_{oc})/2kT} - e^{-q(V-V_{oc})/2kT}), \qquad (3)$$

which is simply the $J(V)$ response of the isolated catalyst-solution circuit element, shifted by V_{oc}. The dependence of Eq. (3) on $J_{o,cat}$ shows why the curves shift to the right as $J_{o,cat}$ is decreased [Fig. 2(a)]. When the bias is high enough that $J \approx J_{ph}$, V_{cat} must increase as $J_{o,cat}$ decreases to maintain the photocurrent J_{ph} [Fig. 2(b)]. Measured V_{cat} data for a metallic nanocrystalline IrO_x catalyst [10] agree with the predictions in Fig. 2(b).

We now discuss adaptive catalysts. The expression for the current between semiconductor and catalyst is [9]

$$J_{jxn} = k_p(p_s - \bar{p}_s e^{qV_{cat}/kT}) - k_n(n_s - \bar{n}_s e^{-qV_{cat}/kT}). \qquad (4)$$

This is similar to the metal-semiconductor current Eq. (1), but where the catalyst potential can now change, altering the density of filled and unfilled catalyst states at the valence and conduction band energies. This causes the reverse currents to depend on V_{cat}, in contrast to the constant reverse currents found in the metallic model [Eq. (1)]. The catalyst-solution current Eq. (2) remains the same.

Simulations were performed for a range of $J_{o,cat}$ values [Figs. 2(c) and 2(d)]. The $J(V)$ response [Fig. 2(c)] is now close to the photodiode response over a larger range of $J_{o,cat}$ values than the metallic catalyst response is. This indicates that adaptive catalysts are capable of higher efficiency than metallic ones when $J_{o,cat}$ is small enough that a significant overpotential is required to maintain the photocurrent.

Figure 2(d) shows that as $J_{o,cat}$ is decreased, V_{cat} increases, while the $J(V)$ response in Fig. 2(c) remains the same. In this regime, the catalyst becomes more oxidized to compensate for decreases in $J_{o,cat}$ and thus maintains the same current. As $J_{o,cat}$ is decreased further, E_{cat} eventually reaches the hole quasi-Fermi level $E_{F,p}$ [Fig. 3(a)]. $E_{F,p}$ and E_{cat} then move toward E_V^s together, leading again to the same $J(V)$ response, in this case because p_s is now increasing to maintain the current and compensate for decreasing $J_{o,cat}$. Finally, at low enough $J_{o,cat}$ values, p_s cannot further increase because $E_{F,p}$ approaches E_V^s, leading to a positive shift in the photocurrent onset [Fig. 2(c)]. The rapid change of V_{cat} near $V = V_{oc}$ is seen in both simulation and experimental data with ion-permeable catalysts [Fig. 2(d)].

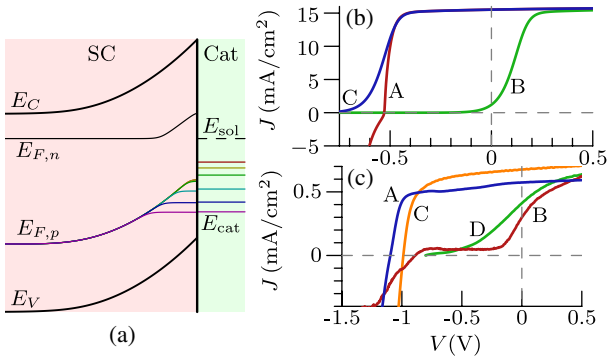

FIG. 3 (color online). (a) Band diagram from adaptive model simulations showing the semiconductor-catalyst interface at short circuit ($V = 0$) under illumination, with each color representing a different $J_{o,cat}$ from 1.4×10^{2} to 1.4×10^{-4} mA cm^{-2} in steps of 10. (b) $J(V)$ responses for the adaptive (curve A) and metallic (curve B) models with $J_{o,cat} = 1.4 \times 10^{-2}$ mA cm^{-2} and $\phi_b = 1$ eV. Curve C shows the metallic model response in which ϕ_b has been increased to the effective barrier ϕ_b^{eff} [Eq. (5)]. (c) Measured $J(V)$ responses for permeable hydrated $IrO_x \cdot (H_2O)_x$ and $Ni(OH)_2/NiOOH$ (curves A and C) compared to impermeable nanocrystalline IrO_x and NiO_x (curves B and D) catalysts on n-TiO_2 [9].

The better performance of adaptive catalysts is a consequence of the system behaving as a single circuit element instead of two separate elements joined by a metallic conductor. With adaptive catalysts, free motion of ions causes the entire electrostatic potential to drop across the semiconductor; n_s is therefore always smaller with adaptive catalysts than with metallic ones (due to increased band bending), leading to less forward electron current and a larger voltage at the maximum power point.

Another way to understand the improved performance is by the notion of an "effective" barrier height. Figure 3(b) shows $J(V)$ responses of the adaptive (curve A) and metallic (curve B) models with $J_{o,cat} = 1.4 \times 10^{-2}$ mA cm^{-2} and $\phi_b = 1$ eV. With these parameters, the adaptive model yields $V_{cat} \approx 0.65$ V when $J \approx J_{ph}$. Because V_{cat} is the difference between E_{sol} and E_{cat}, its value can be interpreted as the increase in the effective barrier at the adaptive catalyst-semiconductor interface during operation relative to the fixed barrier height at the metallic interface. Increasing the barrier at the metallic catalyst-semiconductor interface by 0.65 eV to match the effective barrier of the adaptive system $\phi_b^{eff} = 1.65$ eV gives curve C in Fig. 3(b). Curve C overlaps curve A until near V_{oc} and their maximum power points are nearly identical.

These simulations show that when $J_{o,cat} \ll J_{ph}$, photoelectrodes with adaptive catalysts have the same efficiency as those with metallic catalysts in which the barrier height has been increased to the effective value [9]

$$\phi_b^{eff} \approx \phi_b + (2kT/q)\ln(J_{ph}/J_{o,cat}). \quad (5)$$

Equation (5) holds until $E_{F,p}$ approaches E_V^s, leading to a substantial reverse hole current that counteracts the photocurrent. To compare with simulations, catalysts were prepared in ion-permeable and impermeable forms [9] and their $J(V)$ responses measured [Fig. 3(c)]. The effective barrier height shift is also observed in the experimental data.

We now discuss molecular catalysts. The catalyst-solution current is modeled as a second-order molecular reaction, $C^+ + R \leftrightharpoons C + O$, where C^+ and C are the concentrations of the oxidized and neutral catalyst sites, respectively. This leads to the catalyst-solution current [9]

$$J_{cat} = k_{cat}C^+ - k'_{cat}C = k_{cat}\hat{C}\frac{e^{qV_{cat}/kT} - 1}{e^{qV_{cat}/kT} + K}, \quad (6)$$

where k_{cat}, k'_{cat} are the pseudo-first-order forward and reverse rate constants (since O and R are constant), $K \equiv k_{cat}/k'_{cat} = e^{-(E^o_{cat} - E_{sol})/kT}$ is the equilibrium constant for the reaction, and $\hat{C}$ is the total catalyst site concentration.

The semiconductor-catalyst current is modeled using second-order reactions,

$$p_s + C \leftrightharpoons \{p_s\} + C^+, \quad (7)$$

$$n_s + C^+ \leftrightharpoons \{n_s\} + C, \quad (8)$$

where $\{p_s\}$ and $\{n_s\}$ represent unoccupied surface hole and electron states, respectively, which are assumed constant. Kinetic theory gives the total current

$$J_{jxn} = (k_p^m p_s C - k_p^{m\prime}\{p_s\}C^+) - (k_n^m n_s C^+ - k_n^{m\prime}\{n_s\}C), \quad (9)$$

where k_p^m, $k_p^{m\prime}$ are the forward and reverse rate constants for the reaction in Eq. (7) and k_n^m, $k_n^{m\prime}$ are the forward and reverse rate constants for the reaction in Eq. (8). $k_p^{m\prime}\{p_s\}$ and $k_n^{m\prime}\{n_s\}$ can be related to k_p^m and k_n^m using detailed balance [9].

The results are shown in Figs. 2(e) and 2(f). The molecular catalysts are assumed to have only one oxidized and one reduced state. Thus, when k_{cat} is small and $V \gg V_{oc}$, C^+ approaches $\hat{C}$, and the current is limited by the rate at which the fully oxidized catalyst can oxidize the solution, $J \approx k_{cat}\hat{C}$. For small k_{cat} and $V \ll V_{oc}$, C approaches $\hat{C}$, and the current is limited by the rate at which the solution can oxidize the catalyst, $J \approx -k_{cat}K^{-1}\hat{C}$. When k_{cat} is large, the $J(V)$ response is that of the photodiode.

To enable direct comparison of the molecular and previous models, we chose values of k_{cat} that produce the same exchange currents as the other models [i.e., $k_{cat} = J_{o,cat}(1 + K)/\hat{C}$ [9]]. For comparable values of k_{cat} and $J_{o,cat}$, photoelectrodes with molecular catalysts outperform metallic ones as long as the catalyst does not become saturated. As with adaptive catalysts, E_{cat} for molecular catalysts can change (in this case, by altering C^+/C), thus forming another type of adaptive barrier. In general, however, molecular catalysts are not as efficient as adaptive ones, because the limited number of available unoxidized catalyst sites constrains the degree to which V_{cat} can increase while maintaining sufficiently large C such that hole transfer from semiconductor to catalyst does not decrease the current.

In conclusion, we have shown that the commonly employed equivalent circuit model [4,13–16] containing a photodiode in series with a catalyst-solution system [Fig. 1(a)] is inadequate to describe the $J(V)$ behavior of SCS systems with ion-permeable catalysts; unified models with appropriate boundary conditions are required. The lower efficiency of photoelectrodes with metallic catalysts relative to adaptive or molecular ones originates from the metal-semiconductor interface that is spatially separated from the catalyst-solution interface. Because of the boundary condition at the metal-semiconductor interface Eq. (1), the semiconductor interacts with the catalyst only through the division of the potential drops V_{jxn} and V_{cat}. Boundary conditions consistent with ion-permeable catalysts produce "adaptive" semiconductor-catalyst

barriers and thus higher efficiency. Understanding interfaces with redox-active ion-permeable catalysts is particularly important given the high OER activity of Co and Ni based ion-permeable oxyhydroxides [3–5,14], which, consistent with our theory, also appear to yield the highest performance water-oxidizing photoanodes [7,10,25]. Our recent experiments using n-TiO_2 revealed adaptive barriers with ion-permeable $Ni(OH)_2/NiOOH$ and constant barriers with ion-impermeable nanocrystalline IrO_x catalysts [10].

Finally, we note that we have limited the simulations to extremes in the catalyst models: those with a continuum of electronic states (metallic and adaptive catalysts) and those with a single electronic state (molecular catalysts), as well as completely ion-permeable and impermeable catalysts. Many catalysts likely lie between these extremes. The substantial differences we discovered demonstrate that a complete microscopic picture of SCS systems requires consideration of the physical and electronic properties of the catalyst. Understanding the role of ion permeability and electronic DOS in charge transfer at catalyst-semiconductor interfaces is important in elucidating the behavior of SCS devices and their operational mechanisms.

This work was supported by the DOE Basic Energy Sciences, Grant No. DE-FG02-12ER16323.

*swb@uoregon.edu

[1] M. G. Walter, E. L. Warren, J. R. McKone, S. W. Boettcher, Q. Mi, E. A. Santori, and N. S. Lewis, Chem. Rev. **110**, 6446 (2010).
[2] D. R. Gamelin, Nat. Chem. **4**, 965 (2012).
[3] B. Klahr, S. Gimenez, F. Fabregat-Santiago, J. Bisquert, and T. W. Hamann, J. Am. Chem. Soc. **134**, 16693 (2012).
[4] L. Trotochaud, T. J. Mills, and S. W. Boettcher, J. Phys. Chem. Lett. **4**, 931 (2013).
[5] K. Sivula, J. Phys. Chem. Lett. **4**, 1624 (2013).
[6] M. Barroso, C. A. Mesa, S. R. Pendlebury, A. J. Cowan, T. Hisatomi, K. Sivula, M. Grätzel, D. R. Klug, and J. R. Durrant, Proc. Natl. Acad. Sci. U.S.A. **109**, 15640 (2012).
[7] T. W. Kim and K.-S. Choi, Science **343**, 990 (2014).
[8] H. Reiss, J. Electrochem. Soc. **125**, 937 (1978).
[9] See Supplemental Material at http://link.aps.org/supplemental/10.1103/PhysRevLett.112.148304 for detailed descriptions of the models and simulations.
[10] F. Lin and S. W. Boettcher, Nat. Mater. **13**, 81 (2014).
[11] K. Kinoshita, *Electrochemical Oxygen Technology*, The Electrochemical Society Series (Wiley, New York, 1992).
[12] S. W. Boettcher *et al.*, J. Am. Chem. Soc. **133**, 1216 (2011).
[13] M. R. Shaner, K. T. Fountaine, and H.-J. Lewerenz, Appl. Phys. Lett. **103**, 143905 (2013).
[14] Y. Surendranath, D. K. Bediako, and D. G. Nocera, Proc. Natl. Acad. Sci. U.S.A. **109**, 15617 (2012).
[15] M. T. Winkler, C. R. Cox, D. G. Nocera, and T. Buonassisi, Proc. Natl. Acad. Sci. U.S.A. **110**, E1076 (2013).
[16] P. G. Santangelo, G. M. Miskelly, and N. S. Lewis, J. Phys. Chem. **92**, 6359 (1988).
[17] L. Trotochaud, J. K. Ranney, K. N. Williams, and S. W. Boettcher, J. Am. Chem. Soc. **134**, 17253 (2012).
[18] J. G. McAlpin, T. A. Stich, W. H. Casey, and R. D. Britt, Coord. Chem. Rev. **256**, 2445 (2012).
[19] R. Subbaraman, D. Tripkovic, K.-C. Chang, D. Strmcnik, A. P. Paulikas, P. Hirunsit, M. Chan, J. Greeley, V. Stamenkovic, and N. M. Markovic, Nat. Mater. **11**, 550 (2012).
[20] F. Lin, E. M. Walker, and M. C. Lonergan, J. Phys. Chem. Lett. **1**, 720 (2010).
[21] N. Sato, *Electrochemistry at Metal and Semiconductor Electrodes* (Elsevier, Amsterdam, 1998).
[22] P. Delahay, *Double Layer and Electrode Kinetics* (Interscience, New York, 1965).
[23] C. L. Anfuso, R. C. Snoeberger, A. M. Ricks, W. Liu, D. Xiao, V. S. Batista, and T. Lian, J. Am. Chem. Soc. **133**, 6922 (2011).
[24] M. Gratzel, Nature (London) **414**, 338 (2001).
[25] S. D. Tilley, M. Cornuz, K. Sivula, and M. Grätzel, Angew. Chem., Int. Ed. **49**, 6405 (2010).